

DECONVOLUTION USING THE ADAPTIVE SELECTIVE SIDELOBE CANCELLER BEAMFORMER

Ronny Levanda* and Amir Leshem

Faculty of Engineering, Bar-Ilan University, 52900, Ramat-Gan, Israel

ABSTRACT

We propose a new sequential deconvolution algorithm, that is applicable to imaging using moving and synthetic aperture arrays. The new method results in a higher resolution and a more accurate estimation than commonly used methods when strong interfering sources are present inside and outside the field of view (terrestrial interference, confusing sources). We demonstrate the algorithm performance over both simulated and real radio astronomical data.

Index Terms— Radio astronomy, synthetic aperture, deconvolution, CLEAN, dynamic range, terrestrial, interference, algorithm, ASSC, adaptive selective sidelobe canceller.

1. INTRODUCTION

Observing weak sources in the surroundings of interfering sources is one of the main challenges facing aperture synthesis imaging in radio astronomy. Aperture synthesis, uses a sensor array (or antenna array) that receives the signal at a series of epochs (i.e., the measurement time) and the different measurements from all epochs are combined to obtain the estimation. This problem also appears for instance in radar imaging, [1], [2].

When the field-of-view (FOV) contains radiating sources in the surroundings of the signal-of-interest (SOI), which is often the case, these sources, can interfere via the array sidelobes and affect the estimation of the SOI. In some instances, the interfering sources are significantly stronger than the SOI; in others, the interfering sources are close to the SOI (i.e., the angular distance between the SOI and the interfering sources is small). This may result in an inferior and inaccurate power and location estimation of the SOI. In more extreme cases, the ability to detect the SOI may be lost. To overcome these problems, a variety of *interference mitigation techniques* are employed.

One approach to mitigating interference, is to increase the resolution of the estimated image for a single measurement of the array (i.e., a single correlation matrix) using a beamformer with adaptive weights. Resolution enhancement uses adaptive

beamformers such as multiple-signal-classification (MUSIC), minimum-variance-distortionless-response (MVDR) which is also known as the Capon beamformer, and the adaptive-angular-response (AAR). The MUSIC beamformer (see [3–5]) calculates the estimated direction-of-arrival (DOA) of the source with high resolution. It is applicable to situations where the number of sources is smaller than the number of sensors (or antennas) in the array. Therefore it cannot be used in applications with more sources than receiving elements (such as radio astronomy). The MVDR weights are set to minimize the incoming power while passing the SOI undistorted (see [3] and [6]). The MVDR achieves an enhanced resolution and can be used even in multiple source scenarios. The MVDR beamformer was first suggested for radio astronomy applications, by Leshem and van der Veen at [7], [8] and further developed in [9–11].

Another approach to removing the effect of sidelobes and of strong sources is the *Deconvolution* algorithm applied in radio astronomy. The estimated image (using either the Bartlett, MVDR or AAR weights) is the basis for further processing which enhances the estimation accuracy for noisy images and images with high dynamic range. The most widely used deconvolution algorithms are CLEAN (proposed by Högbom [12]) and MEM (Maximal Entropy Method, see [13–16]). The CLEAN algorithm assumes that the observed field of view is composed of point sources. CLEAN iteratively removes the brightest point source from the image until the residual image is noise-like. The point sources are accumulated during the iteration and the reconstructed image is the accumulated source list convolved with a reconstruction beam (usually a Gaussian). During the iterations, CLEAN subtracts the strongest point sources from the data. A multi-scale CLEAN proposed by Cornwell [17] models the brightness of the sky as the sum of the components of the emission that have different size scales. Extensions of the CLEAN algorithm to support wavelets as well as non-co-planar arrays were reviewed by Rau et al. [18] and the W-projection was proposed by Cornwell et al. [19]. For interference dominant scenarios, the interfering source is removed from the image to enable detection and estimation (power and DOA) of the SOI. The proposed algorithm, obtains an image with a higher resolution for every step in the deconvolution algorithm; to yield a final estimation with better accuracy.

* Email: ronny.levanda@gmail.com

This research was supported by ISF grant 1240/09: Signal processing and imaging for large radio telescopes.

For cases where the interfering source is outside the FOV and is significantly stronger than the sources in the FOV, the interfering source is observed separately, and then an image with larger FOV is estimated using a *mosaicing* algorithm (see [20]), to enable the CLEAN algorithm to estimate and subtract the interfering source from the image.

The standard approach to combining different array measurements is averaging (see [21], [7] and [22]).

Our approach is to minimize the undesired interference radiation received through the array sidelobes using the sidelobe variation as a function of time. For each observation angle (a specific pixel in the image), we choose the correlation matrices that minimize the interference. In this sense, our proposed algorithm is a generalization of the MVDR for many array measurements.

In previous work [22, 23] we proposed a new form of dirty image called the Adaptive Selective Sidelobe Canceller (ASSC). In this paper we focus on the radio astronomy application and extend the ASSC dirty image into a full deconvolution algorithm, by combining it with a sequential source removal technique in the visibility domain. It should be emphasized that one of the key issues in this combination is the inclusion of more and more matrices as the deconvolution algorithm continues and the strong sources are removed from the visibility.

The structure of this paper is as follows: In Section (2) we formulate the imaging problem. Section (3) contains a detailed description of the proposed algorithm, deconvolution using the ASSC. Simulated examples, demonstrating the ASSC performance and comparisons to the standard methods is given in Section (4), and Section (5) demonstrates the performance of the proposed algorithm on a real radio telescope data.

2. PROBLEM FORMULATION

Radio Telescopes observation method is based on correlations between the signals received at antenna pairs. Assuming that the observed image is a collection of D point sources, with intensities, $I(l_1, m_1), I(l_2, m_2), \dots, I(l_D, m_D)$, and the correlation matrix (visibility) $\hat{\mathbf{R}}_k$ is measured for time epochs k , $k = 1 \dots K$, the imaging model can be written as (see [22] and [7]),

$$\mathbf{R}_k = \mathbf{A}_k \mathbf{B} \mathbf{A}_k^H + \sigma^2 \mathbf{I} \quad (1)$$

Where \mathbf{R}_k is the correlation matrix at time epoch k , \mathbf{A}_k is defined as

$$\mathbf{A}_k \equiv [\mathbf{a}_k(l_1, m_1), \dots, \mathbf{a}_k(l_D, m_D)], \quad (2)$$

$\mathbf{a}_k(l_i, m_i)$ is the array steering vector toward the i 'th source, (l, m) are the direction cosines, \mathbf{B} is given by

$$\mathbf{B} \equiv \begin{bmatrix} I(l_1, m_1) & & 0 \\ & \ddots & \\ 0 & & I(l_D, m_D), \end{bmatrix} \quad (3)$$

and σ^2 is the noise variance.

This formalism was first proposed in [8] and [7] to allow for the introduction of interference mitigation techniques in the imaging process. It was extended to noncoplanar array and polarimetric imaging in [9]. This formulation also allows the easy inclusion of space-dependent calibration parameters [24].

3. DECONVOLUTION WITH THE ADAPTIVE-SELECTIVE-SIDELOBES-CANCELLER ALGORITHM

The performance (DOA accuracy, dynamic range, spatial resolution) of any deconvolution algorithm is limited by the dirty image resolution and accuracy during the iterations.

During each iteration, the ASSC algorithm, takes, per incident angle, the estimation of the array (time epoch) that *estimates the minimal intensities*. Combining the ASSC methodology with iterative source subtraction, can yield significantly better deconvolution, especially when strong interfering sources affect the image.

We now describe, step by step the ASSC based deconvolution.

1. Initialization:

- (a) Calculate the ASSC initial dirty image $\hat{I}^{ASSC}(l, m)$ as follows,
 - i. Calculate the array output power for *each epoch separately* according to the desired beamformer weight vector, \mathbf{w}_k , by

$$\hat{I}_k(l, m) = \mathbf{w}_k^H(l, m) \mathbf{R}_k \mathbf{w}_k(l, m). \quad (4)$$

- ii. Determine the value of the ASSC parameter, \tilde{k} , where \tilde{k} is the number of the best epochs to consider for a specific observation direction, $1 \leq \tilde{k} \leq K$. The value is set according to a rough evaluation of the interference level at the image (originated by either in FOV or out of FOV interfering sources).

Following [23], we choose only epochs where interference is minimal to the given specific pixel. This is given by

$$\tilde{k} = \begin{cases} K & \alpha_{q_{dB}} < -10\text{dB} \\ p_1 + p_0 \alpha_{q_{dB}} & -10\text{dB} \leq \alpha_{q_{dB}} \leq 15\text{dB} \\ 1 & 15\text{dB} \leq \alpha_{q_{dB}} \end{cases}, \quad (5)$$

where $p_0 = -\frac{K-1}{25}$, $p_1 = K + 10p_0$ and $\alpha_{q_{dB}}$ is the evaluated interference level given in dB. For more details and examples of the optimal \tilde{k} as a function of the interference level, see [23].

- iii. For each (l, m) , (each pixel in the image), find the smallest \tilde{k} values out of all measurements, $\hat{I}_k^{\text{init}}(l, m), k = 1 \dots K$,

$$[\hat{I}_{(1)}^{\text{init}}(l, m), \hat{I}_{(2)}^{\text{init}}(l, m), \dots, \hat{I}_{(\tilde{k})}^{\text{init}}(l, m)], \quad (6)$$

where $\hat{I}_{(k)}^{\text{init}}(l, m)$ is the k 'th smallest elements in the order statistics of $[\hat{I}_1^{\text{init}}(l, m), \dots, \hat{I}_K^{\text{init}}(l, m)]$. i.e., $\hat{I}_{(1)}^{\text{init}}(l, m)$ is the minimal value out of $[\hat{I}_1^{\text{init}}(l, m), \dots, \hat{I}_K^{\text{init}}(l, m)]$ and $\hat{I}_{(K)}^{\text{init}}(l, m)$ is the maximal value.

- iv. The ASSC initial dirty image is given by,

$$\hat{I}_{\text{init}}^{\text{ASSC}}(l, m) = \frac{1}{\tilde{k}} \sum_{k=1}^{\tilde{k}} \hat{I}_{(k)}^{\text{init}}(l, m). \quad (7)$$

- (b) set the loop gain parameter, γ , (typically 0.1)
(c) initialize the source list to an empty list. During each deconvolution iteration, a new entry is added to the source list containing the source location and intensity estimate $[l_o^n, m_o^n, s_o^n]$ (where n is the iteration number).

2. Find the brightest source in the dirty image

$$(l_o^n, m_o^n) = \arg \max_{l, m} \hat{I}^{\text{ASSC}}(l, m), \quad (8)$$

add a new entry to the source list with the location and intensity estimate of the new source, $[l_o^n, m_o^n, s_o^n]$, and remove a fraction of it from the visibility data,

$$\begin{aligned} \mathbf{R}_k &= \mathbf{R}_k - \gamma s_o^n \mathbf{a}_k(l_o^n, m_o^n) \mathbf{a}_k^H(l_o^n, m_o^n), \\ &\forall k = 1, \dots, K \end{aligned} \quad (9)$$

Where γ is the loop gain parameter, s_o^n is the estimated source intensity, \mathbf{a}_k is the arrays steering vector and \cdot^H stands for the hermitian conjugate.

3. Update the ASSC parameter \tilde{k} according to the current interference level, α_q dB, according to Equation (5). note, for a high interference level inside the FOV, the ASSC parameter \tilde{k} will start at $\tilde{k} = 1$ for the first iterations, and will increase at value to $\tilde{k} = K$ as the iterations remove the strong interfering sources.

4. Update the ASSC dirty image, $\hat{I}^{\text{ASSC}}(l, m)$ by,

$$\hat{I}^{\text{ASSC}}(l, m) = \frac{1}{\tilde{k}} \sum_{k=1}^{\tilde{k}} \hat{I}_{(k)}(l, m), \quad (10)$$

where $I_{(k)}(l, m)$ is the k 'th order statistics of $\{I_1, I_2, \dots, I_K\}$, calculated using the new \mathbf{R}_k matrices

$$\hat{I}_k(l, m) = \mathbf{w}_k^H(l, m) \mathbf{R}_k \mathbf{w}_k(l, m). \quad (11)$$

5. Repeat steps (2) through (4) until the residual image, $\hat{I}^{\text{ASSC}}(l, m)$ is noise like.

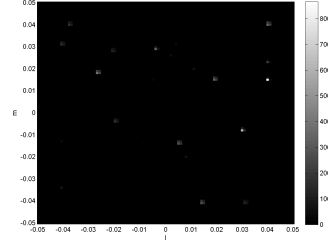


Fig. 1. Simulated sky true image

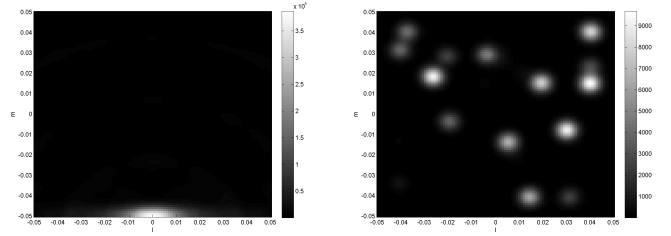


Fig. 2. Reconstructed image of: the existing CLEAN algorithm on the left. The image is corrupted due to the out-of-FOV radiating object. On the right ASSC based deconvolution. Sources are reconstructed, and the out-of-FOV object's radiation is suppressed.

6. Produce the image reconstruction from the accumulated source list

$$I(l, m) = \sum_n \gamma s_o^n \mathbf{B}_{\text{synth}}(l - l_o^n, m - m_o^n). \quad (12)$$

Where $\mathbf{B}_{\text{synth}}$ is the synthesize beam, usually a Gaussian, (l_o^n, m_o^n) are the sources location at the n 'th iteration, s_o^n are their intensities and γ is the loop gain.

The computational complexity of the ASSC beamformer is similar in complexity to the standard method (using the same weights), with the following minor modification: for each pixel, find the \tilde{k} minimal powers from $[\hat{I}_1(l, m), \dots, \hat{I}_K(l, m)]$.

4. SIMULATED EXAMPLE

This section illustrates the performance of the ASSC based deconvolution using the MVDR weights, compared with the standard CLEAN algorithm. The test case is produced using a radio-telescope simulation of a linear array with 30 antennas, logarithmic spaced up to 200λ , and includes thermal noise at the antennas. Measurement was done every half a minute for 12 hours.

The simulated sky (see Figure (1)) contains a collection of point sources with various intensities and an out-of-FOV strong interfering source. The out-of-FOV source, located at

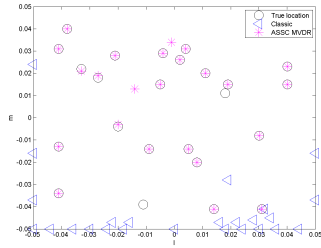


Fig. 3. DOA estimation of the multiple source with a strong out-of-FOV interfering source. The standard method failed to reconstruct the true sources in the image, whereas the ASSC based algorithm reconstructed most sources.

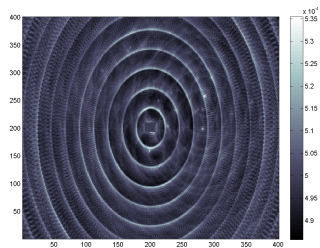


Fig. 4. Classic initial dirty image of the quasar observation after graphically suppressing the center source’s intensity (i.e., the color-map is adjusted to the faint sources and the side-lobes, see text for more details). A few of the faint sources are clearly seen at the image together with the side-lobes of the strong source.

$(l, m) = (0, -0.06)$, intensity is stronger by a factor of 5×10^4 from the strongest source in the FOV.

Figure (2) shows the reconstructed images using the traditional CLEAN and the ASSC based deconvolution using the MVDR weights. Due to the out-of-FOV radiating sources, the standard method fails to reconstruct the true sources. The reconstructed image only shows the sidelobes of the interfering source. In a ‘real life’ scenario, dealing with such a strong out-of-FOV interference would require mosaic. As opposed to the standard method, the ASSC based algorithm, manages to reconstruct most observed sources, suppressing the out-of-FOV source sidelobes. The estimated DOA of the two algorithms is shown in Figure (3). The 30 strongest sources detected by the standard method are due to the out-of-FOV interfering sources sidelobes, whereas the ASSC based algorithm reconstructed most of the true sources.

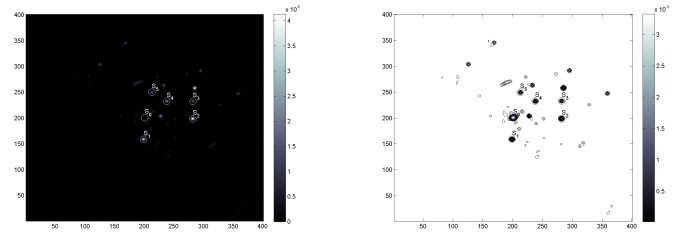


Fig. 5. CLEAN using the ASSC MVDR - reconstructed image after 400 iterations (left). The same image is shown in contour plot at the right. Identified sources are marked by circles (see text for more details).

5. EXAMPLE OF THE VARIATING QUASAR J1819+3845

The Quasar *J1819 + 3845* was observed using the Westerbork Synthesis Radio Telescope (WSRT) by A.G. de Bruyn¹. Observation was done at a wavelength of 1.4GHz and 64 frequency bins were measured, each of width of 312KHz.

The measurement set contains visibility measurements of 64 frequencies, each with 1438 epochs, a total of 92032 ($64 \cdot 1438$) visibility matrices were measured. Analysis was done for the center 50 frequency bins (selected bin range is 5 – 54) and 120 epochs (every 12’lv was selected). The analysis included an overall of 6000 visibility matrices (each measured at a different epoch or a different frequency).

The classic initial dirty images is shown in Figure (4). Since the strong Quasar at the center of the image does not allow the faint source intensities to be seen, the center of the image was padded with the median value of the image (overwriting the strong source intensity) and a few of the sources are clearly seen.

The CLEAN results after 400 CLEAN iterations using the proposed algorithm (ASSC with MVDR weights) are given in Figure (5). All apparent true sources are detected by the algorithm in addition to a weaker sources that are not seen at the original dirty image. Identified sources specified by de Bruyn and Macquart [25], are marked by circles and the letters $S_0 - S_5$ (note, at the left image, the strong quasar intensity marked by S_0 , was graphically removed to enable the fainter sources to be seen).

6. SUMMARY

In this paper, we presented a new deconvolution algorithm, based on the interference minimization philosophy of the adaptive selective sidelobe canceller, and demonstrated its performance over a synthetic and a real radio astronomical data examples.

¹We would like to thank A. Ger de Bruyn for all his assistance and for sharing the data with us.

References

- [1] J. Li, R. Wu, and V.C. Chen, "Robust autofocus algorithm for ISAR imaging of moving targets," *Aerospace and Electronic Systems, IEEE Transactions on*, vol. 37, no. 3, pp. 1056–1069, Jul 2001.
- [2] R.B. Wu, Z.S. Liu, and J. Li, "Time-varying complex spectral estimation with applications to ISAR imaging," in *Signals, Systems and Computers, 1998. Conference Record of the Thirty-Second Asilomar Conference on*, Nov. 1998, vol. 1, pp. 14–18 vol.1.
- [3] H. Van Trees, *Optimum array processing*, J. Wiley, 2002.
- [4] R. O. Schmidt, "Multiple emitter location and signal parameter estimation," *IEEE Trans. Antennas Propagation*, pp. 276–280, Mar. 1986.
- [5] G. Bienvenu and L. Kopp, "Optimality of high resolution array processing using the eigensystem approach," *IEEE Trans. Acoust., speech, signal process.*, pp. 1234–1248, Oct. 1983.
- [6] J. Capon, "High resolution frequency-wavenumber spectrum analysis," *Proceedings of the IEEE*, pp. 1408–1418, 1969.
- [7] A. Leshem and A.J. van der Veen, "Radio-astronomical imaging in the presence of strong radio interference," *IEEE Trans. on Information Theory, Special issue on information theoretic imaging*, pp. 1730–1747, August 2000.
- [8] A. Leshem, A.J. van der Veen and A. J. Boonstra, "Multichannel interference mitigation techniques in radio-astronomy," *The Astrophysical Journal Supplements*, pp. 355–373, November 2000.
- [9] Chen Ben-David and A. Leshem, "Parametric high resolution techniques for radio astronomical imaging," *IEEE Journal of Selected Topics in Signal Processing*, vol. 2, no. 5, pp. 670–684, Oct. 2008.
- [10] J. Raza, A.J. Boonstra and A.J. van der Veen, "Spatial filtering of RF interference in radio astronomy," *IEEE Signal Processing Letters*, vol. 9, pp. 64, 2002.
- [11] B.D. Jeffs, L. Li and K.F. Warnick, "Auxiliary antenna-assisted interference mitigation for radio astronomy arrays," *IEEE Transactions on Signal Processing*, vol. 53, pp. 439, 2005.
- [12] J. A. Högbom, "Aperture synthesis with nonregular distribution of interferometer baselines," *Astron. Astrophys. Suppl.*, vol. 15, pp. 417–426, 1974.
- [13] B.R. Frieden, "Restoring with maximum likelihood and maximum entropy," *Journal of the Optical Society of America*, vol. 62, pp. 511–518, 1972.
- [14] S.F. Gull and G.J. Daniell, "Image reconstruction from incomplete and noisy data," *Nature*, vol. 272, pp. 686–690, 1978.
- [15] J.G. Ables, "Maximum entropy spectral analysis," *AAS*, vol. 15, pp. 383–393, 1974.
- [16] S.J. Wernecke, "Two dimensional maximum entropy reconstruction of radio brightness," *Radio Science*, vol. 12, pp. 831–844, 1977.
- [17] T.J. Cornwell, "Multiscale CLEAN deconvolution of radio synthesis images," *IEEE Journal of Selected Topics in Signal Processing*, vol. 2, no. 5, pp. 793–801, Oct. 2008.
- [18] U. Rau, S. Bhatnagar, M.A. Voronkov, and T.J. Cornwell, "Advances in calibration and imaging techniques in radio interferometry," *Proceeding of the IEEE*, vol. 97, pp. 1472–1481, Aug. 2009.
- [19] T.J. Cornwell, K. Golap, and S. Bhatnagar, "The non-coplanar baselines effect in radio interferometry: The w-projection algorithm," *IEEE Journal of Selected Topics in Signal Processing*, vol. 2, no. 5, pp. 647–657, October 2008.
- [20] G.B. Taylor, C.L. Carilli, and R.A. Perley, *Synthesis Imaging in Radio-Astronomy*, Astronomical Society of the Pacific, 1999.
- [21] D. Rieken and D. Fuhrmann, "Generalizing MUSIC and MVDR for multiple noncoherent arrays," *IEEE Trans. on Signal Processing*, vol. 52, pp. 2396–2406, Sept. 2004.
- [22] R. Levanda and A. Leshem, "Synthetic aperture radio telescopes," *IEEE Signal Processing Magazine*, vol. 27, pp. 14–29, Jan. 2010.
- [23] R. Levanda and A. Leshem, "Adaptive selective side-lobe canceller beamformer with applications to interference mitigation in radio astronomy," *Signal Processing, IEEE Transactions on*, vol. 61, no. 20, pp. 5063–5074, 2013.
- [24] S. van der Tol, *Bayesian Estimation for Ionospheric Calibration in Radio Astronomy*, Ph.D. thesis, Delft University of Technology, 2009.
- [25] A.G.de Bruyn and J.P. Macquart, "The intra-hour variable quasar j1819+3845: 13-year evolution, jet polarization structure and interstellar scattering screen properties," 2014.